STEM CELLS AND DEVELOPMENT
Volume 25, Number 10, 2016

DOI: 10.1089/scd.2015.0335

Increased Expression of EGR-1 in Diabetic Human Adipose Tissue-Derived Mesenchymal Stem Cells Reduces Their Wound Healing Capacity

Nhu-Thuy Trinh,[1] Toshiharu Yamashita,[1] Kinuko Ohneda,[2] Kenichi Kimura,[1] Georgina To'a Salazar,[1] Fujio Sato,[3] and Osamu Ohneda[1]

The prevalence of type 2 diabetes mellitus (T2DM), which leads to diabetic complications, has been increasing worldwide. The possible applications of T2DM-derived stem cells in cell therapy are limited because their characteristics are still not fully understood. In this study, we characterized adipose tissue-derived mesenchymal stem cells (AT-MSCs) from diabetic patients (dAT-MSCs) and found that insulin receptor substrate-1 (IRS-1) was highly phosphorylated at serine 636/639 in dAT-MSCs. Moreover, we found that early growth response factor-1 (EGR-1) and its target genes of *PTEN* and *GGPS1* were highly expressed in dAT-MSCs in comparison to healthy donor-derived AT-MSCs (nAT-MSCs). We observed impaired wound healing after the injection of dAT-MSCs in the ischemic flap mouse model. The expressions of EGR-1 and its target genes were diminished by small hairpin RNA-targeted EGR-1 (shEGR-1) and treatment with a mitogen-activated protein kinase/extracellular signal-regulated kinase (MAPK/ERK) inhibitor (PD98059). Importantly, dAT-MSCs with shEGR-1 were able to restore the wound healing ability in the mouse model. Interestingly, under hypoxic conditions, hypoxia-inducible factor-1α (HIF-1α) can bind to the EGR-1 promoter in dAT-MSCs, but not in nAT-MSCs. Together, these results demonstrate that the expression of EGR-1 was upregulated in dAT-MSCs through two pathways: the main regulatory pathway is the MAPK/ERK pathway, the other is mediated by HIF-1α through direct transcriptional activation at the promoter region of the *EGR1* gene. Our study suggests that dAT-MSCs may contribute to microvascular damage and delay wound healing through the overexpression of EGR-1. Interrupting the expression of EGR-1 in dAT-MSCs may be a useful treatment for chronic wounds in diabetic patients.

Introduction

The major problems of type 2 diabetes mellitus (T2DM) are associated with cells losing their ability to respond to insulin, which results in poor glucose control and degenerative complications [1,2]. Insulin and chemical treatments, such as sulfonylurea, metformin, thiazolidinedione, exenatide, pramlintide, are useful for achieving the control of T2DM, but difficult to relieve the symptoms of diabetic complications directly [3–5]. Chronic wounds, which occur in one or more phases of wound healing, are a common diabetic complication [6,7]. Hyperglycemia in diabetes leads to blood flow abnormalities, microvascular cell loss, and the lack of trophic factors in endothelial and neuronal cells, which results in hypoxia or ischemia causing tissue disease and degeneration [2,8].

Hypoxia stabilizes an important transcription factor, hypoxia-inducible factor (HIF)-1α, which regulates gene expression under hypoxic conditions [9,10]. Hypoxia-activated cell death leads to impaired endothelial cell barrier function and an increase in vascular permeability, leakage, and necrosis [11,12].

Hypoxia increases the transcriptional activation of early growth response factor-1 (EGR-1), which is highly expressed in the abdominal fat of diabetic patients and in *db/db* mice [13–15]. EGR-1 expression is also mediated through mitogen-activated protein kinase (MAPK), including the extracellular signal-regulated kinase (ERK) pathway [15]. EGR-1 activates the expression of many growth factors such as bFGF and TGF-β, adhesion molecules (Cyr61, ICAM-1, and MCP-1), and theinflammatory signaling cascade of TNF-α and interleukin-6 (IL-6). Thus, high EGR-1 activity is involved in the pathogenesis of atherosclerosis, restenosis, and cardiovascular diseases [16–19]. A previous study demonstrated that atherosclerosis and vascular inflammation were decreased in homozygous Egr-$1^{-/-}$/apo$E^{-/-}$ double-knockout mice [19].

Stem cell therapy has recently shown promise in the prevention of diabetic complications due to its regenerative

[1]Graduate School of Comprehensive Human Science, Laboratory of Regenerative Medicine and Stem Cell Biology and [3]Department of Cardiovascular Surgery, University of Tsukuba, Tsukuba, Japan.
[2]Laboratory of Molecular Pathophysiology, Faculty of Pharmacy, Takasaki University of Health and Welfare, Takasaki, Japan.

potential [20–22]. However, it has been demonstrated that diabetic adipose tissue-derived mesenchymal stem cells (dAT-MSCs) had abnormal gene expression profiles and exhibited a low capacity for differentiation into osteoblasts and chondrocytes in comparison to non-diabetic adipose tissue-derived mesenchymal stem cells (nAT-MSCs) under in vitro conditions that mimicked hyperglycemia [23]. The present study aimed to elucidate the characteristics of dAT-MSCs under normoxic and hypoxic conditions in vitro and in vivo, in a mouse model of wound healing, to allow for a better understanding of the potential future applications of dAT-MSCs in stem cell therapy.

We provide evidence that EGR-1 is highly expressed in dAT-MSCs and that is regulated by both ERK1/2 signal pathway and HIF-1α under normoxic and hypoxic conditions, indicating that the upregulation of EGR-1 affects the functional role of adipose tissue-derived mesenchymal stem cells (AT-MSCs) in diabetic patients. This finding suggests that EGR-1 may be an ideal therapeutic target for improving the function of dAT-MSCs before their therapeutic application.

Materials and Methods

Antibodies

The following antibodies were used for the analyses of stem cell markers: Fluorescein isothiocyanate (FITC)-labeled anti-HLA-ABC (311404; BioLegend), FITC-labeled anti-CD90 (328107; BioLegend), phycoerythrin (PE)-labeled anti-CD13 (301701; BioLegend), PE-labeled anti-CD166 (559263; BD Pharmingen), PE-labeled anti-CD105 (323206; BioLegend), PE-labeled anti-CD73 (550257; BD Pharmingen), PE-labeled anti-HLA-DR (307606; BioLegend), PE-labeled anti-CD31 (303106; BioLegend), PE-labeled anti-CD14 (301806; BioLegend), allophycocyanin (APC)–labeled anti-CD45 (555485; BD Biosciences), and FITC-labeled anti-CD34 (555821; BD Biosciences). APC-labeled anti-IgG1 (555751; BD Biosciences), PE-labeled anti-IgG1 (555749; BD Biosciences), FITC-labeled anti-IgG1 (555748; BD Biosciences) were used as the isotype controls. After staining the nAT-MSCs and dAT-MSCs with fluorochrome-conjugated antibodies, the cells were sorted and analyzed using a MoFlo (MoFlo XDP; Beckman Coulter). The following primary antibodies were used for the western blotting analyses: rabbit mAb Akt (11E7, #4685) and Phospho-Akt (Ser473; (D9E, #4060S); p44/42 ERK1/2 (137F5, #4695) and Phospho-p44/42 ERK1/2 (D13.14.4E, #4370S); rabbit anti-IRS-1 (D23G12) and rabbit antibody phospho-IRS-1 (serine 636/639) (2388) (Cell Signaling Technology); rabbit anti-EGR-1 (588, sc-110); goat anti-β Actin (C-11, sc-1615); goat anti-Lamin B (M20, sc-6217) (Santa Cruz Biotechnology); rabbit anti-HIF-1α (NB100-479; Novus Biologicals); and HRP-conjugated goat anti-rabbit IgG (656120) and rabbit anti-goat IgG (611620) (Invitrogen) were used as the secondary antibodies.

The isolation of AT-MSCs

The studies are performed according to the amended Declaration of Helsinki and all of the experiments were approved by the ethics committee of the University of Tsukuba. Human adipose tissue was obtained after obtaining informed consent from diabetic ($n = 3$, HbA1c >7.0, long-term treatment) and nondiabetic ($n = 3$) donors, male, age = 59 ± 10 years, who were undergoing procedures in the Department of Cardiovascular Surgery, University of Tsukuba Hospital, Tsukuba, Japan. The isolation of AT-MSCs was performed as previously described [24]. Cells were cultured in Iscove's modified Dulbecco's medium (IMDM, 12200-069; Invitrogen), 10% fetal bovine serum, 2 mg/mL L-glutamine (25030; Invitrogen), and 5 ng/mL recombinant human bFGF (064-04541; PeproTech) at 37°C in 5% CO_2 and a humidified atmosphere. After 3 days, the medium containing nonadherent cells was removed and replaced with fresh medium. Frozen cell stocks were prepared using Cell Banker solution (ZENOAQ) and stored in liquid nitrogen for further experiments. All AT-MSCs used for the experiments of this study were at passage 5–8.

The in vitro differentiation of AT-MSCs

In vitro differentiation was performed as described previously [24]. Osteogenic and adipogenic differentiation were assessed on day 21 by 1% Alizarin Red S (Kodak) and Oil Red O (Muto Pure Chemicals) staining, respectively. The final step of assessing the differentiation was to measure absorbance at 482 and 490 nm for Alizarin Red and Oil Red O staining, respectively using a spectrophotometer Gene Quant™100, 4280 V1.6.1 (GE Healthcare). To assess chondrogenic differentiation, cell pellets were sectioned and stained with Hematoxylin and Eosin (H&E; Muto Pure Chemicals) and Toluidine Blue (Muto Pure Chemicals) to visualize the control cells and chondrocytes, respectively. The cells were visualized with an Olympus IX71 microscope (Olympus) under UPlan FI (×10 and ×20). All of the differentiation experiments were performed independently. The nAT-MSC and dAT-MSC experiments were performed in triplicate.

The cell proliferation assay

AT-MSCs were plated at a density of 4×10^4 cells per 35-mm dish, and cultured under normoxic (20% O_2, 37°C) or hypoxic (5% O_2, 37°C) conditions. The cell culture medium was replaced every 4 days. Every 24 h, the cells were washed twice with PBS and dispersed into a single cell solution using 0.05% trypsin/EDTA. The number of cells was counted using Trypan Blue (Invitrogen) exclusion for 10 days.

shRNA transfection

The shRNAs were designed for human EGR-1 (NM_001964, TRCN0000273850; Sigma-Aldrich). The shRNA transfection was performed using the Hexadimethrine Bromide Transfection Reagent (Sigma-Aldrich) according to the manufacturer's protocol.

Insulin stimulation

Insulin stimulation was performed as described previously [14]. nAT-MSCs and dAT-MSCs were cultured under normoxic (20% O_2, 37°C) or hypoxic (5% O_2, 37°C) conditions until cells reached 80% confluence. Insulin (1,000 nM) was added for 1 h to allow for the detection of IRS-1 phosphorylation.

Analysis of ERK1/2 activity in AT-MSCs

nAT-MSCs and dAT-MSCs were cultured in normoxic (20% O_2, 37°C) or hypoxic (5% O_2, 37°C) conditions, until the cells reached 80% confluence. PD98059 (P215; Sigma-Aldrich), an inhibitor of ERK1/2, was used according to the manufacturer's protocol, at a concentration 50 μM for 60 min to detect mRNA expression.

Quantitative reverse transcription polymerase chain reaction

To examine the expression of genes related to osteogenic and adipogenic differentiation, nAT-MSCs and dAT-MSCs were assessed at day 7 after induction. nAT-MSCs and dAT-MSCs were cultured under normoxic (20% O_2, 37°C) or hypoxic (5% O_2, 37°C) conditions for 5 days and RNA was extracted using an RNeasy Mini Kit (Qiagen). Total RNA (1 μg) was reverse transcribed using an reverse transcription polymerase chain reaction (RT-PCR) Kit (TOYOBO). cDNA was analyzed using a GeneAmp 7500 Fast Real-Time PCR System (Life Technologies) using SYBR Green Reagent (TOYOBO). The expression levels of the target genes were analyzed using the ΔΔCt method. The sequences of the primer sets used for the PCR reactions are shown in Table 1.

Western blotting

nAT-MSCs and dAT-MSCs were cultured under normoxic (20% O_2, 37°C) or hypoxic (5% O_2, 37°C) conditions for 4 days. Whole cell lysates were prepared with RIPA buffer (25 mM Tris, 150 mM NaCl, 1% NP-40, 1% sodium deoxycholic acid, 0.1% SDS) for 30 min and centrifuged at 15,000 rpm at 4°C for 10 min. The collected supernatants were used for western blotting analyses. In each group, an equal amount of protein was electrophoresed on 8.5% sodium dodecyl sulfate polyacrylamide gel electrophoresis (SDS-PAGE) gel and then transferred onto PVDF membranes (Immobilon-P; Millipore). The membranes were then incubated with a primary antibody as indicated. HRP-conjugated goat anti-rabbit IgG or rabbit anti-goat IgG was used as secondary antibody, and an enhanced chemiluminescence HRP substrate (Millipore) was used for detection. Goat anti-β-Actin and goat anti-Lamin B were used as the internal controls for monitoring protein loading and transfer.

Enzyme-linked immunosorbent assay

nAT-MSCs and dAT-MSCs were cultured under normoxic (20% O_2, 37°C) or hypoxic (5% O_2, 37°C) conditions for 4 days. Then, cells were treated with PD98059 (50 μM) in fresh culture medium (IMDM) for 60 min. The quantitative concentration of IL-6 present in cell culture supernatants was measured by the IL-6 High Sensitivity Human Enzyme-Linked Immunosorbent Assay (ELISA) Kit (D6050; R&D systems) following the manufacturer's protocol.

Chromatin immunoprecipitation assay

dAT-MSCs were cultured under normoxic (20% O_2, 37°C) or hypoxic (5% O_2, 37°C) conditions for 4 days. A

Table 1. The Primers Used for Quantitative Polymerase Chain Reaction

Function	*Gene*	*Primer*	*Sequence*
Internal control	β-actin	5′-primer	GTGCGTGACATTAAGGAGAAGCTGTGC
		3′-primer	GTACTTGCGCTCAGGAGGAGCAATGAT
Transcription factors	EGR-1	5′-primer	AGTCTTTTCCTGACATCTCTCTGAA
		3′-primer	ACTAGGCCACTGACCAAGCTGAA
Angiogenic factors	TGF-β	5′-primer	AGAGCTCCGAGAAGCGGTACCTGAACCC
		3′-primer	GTTGATGTCCACTTGCAGTGTGTTATCC
	bFGF	5′-primer	AGAGCGACCCTCACATCAAGCTACAAC
		3′-primer	ATAGCTTTCTGCCCAGGTCCTGTTTTG
Adhesion molecules	Cyr61	5′-primer	TGGGTCTGTGACGAGGATAGTATCAAGG
		3′-primer	CTTGTAAAGGGTTGTATCGGATGCGAGG
	Col4	5′-primer	AGGGCCAGCCTGGCCTGCCAGGACTTCC
		3′-primer	TCACCCTTAGAGCCTGTGATTCCTGGAG
	Inav	5′-primer	ATACGACCCCAATGTTTACAGCATCAAG
		3′-primer	GCCAGTAAAATTGTATAAGGAGGACATG
Proinflammatory cytokine	IL-6	5′-primer	ACAAGAGTAACATGTGTGAAAGCAG
		3′-primer	TATACCTCAAACTCCAAAAGACCAG
Adipogenic markers	PPARγ2	5′-primer	GCCAAGGCTTCATGACAAGGGAGTTTC
		3′-primer	CACGTGTTCCGTGACAATCTGTCTGAG
	Adiponectin	5′-primer	CCTGGTGAGAAGGGTGAGAAAGGAGATCC
		3′-primer	TGTGATGTGGTAGGCAAAGTAGTACAGCC
Osteogenic markers	Runx2	5′-primer	CAGATGGGACTGTGGTTACTGTCATGG
		3′-primer	CCTAAATCACTGAGGCGGTCAGAGAAC
	ALP	5′-primer	ACGTGGCTAAGAATGTCATC
		3′-primer	CTGGTAGGCGATGTCCTTA
Mediators of insulin resistance	PTEN	5′-primer	TTG GCG GTG TCA TAA TGT CT
		3′-primer	GCA GAA AGA CTT GAA GGC GTA
	GGPS1	5′-primer	ACTGTTTGGATTAGCAGTAGGTCTC
		3′-primer	GGAGTGTAGATTAGCATAATCATCC

chromatin immunoprecipitation (ChIP) assay was performed using a ChIP-IT Express Enzymatic Kit (Active Motif) according to the manufacturer's instructions. The extracted chromatin samples were enzymatically sheared and immunoprecipitated with rabbit anti-HIF-1α, and control IgG as the primary antibodies. The precipitated genome fragments were subjected to a PCR. The PCR primer set was designed for the HRE sequence on the EGR-1 promoter as follows:

hEGR-1-3k HRE sense—(AGACTTCCACAGGCGAT TCTGCTGC) and antisense—(GCAATTGGCATTCAACA AACAGTGG).

Animal studies

Female C57BL/6 mice were purchased from Charles River Japan, Inc. All of the mice were maintained on a 12-h light–12-h dark cycle in the Animal Research Center of the University of Tsukuba. All protocols of the animal experiments were approved by the Animal Care Committee of the University of Tsukuba. The mouse skin flap model was performed as described previously [25]. Briefly, 10-week-old C57BL/6 mice were anesthetized and a peninsula-shaped incision (3×2 cm) was made on the dorsal surface, generating an ischemia gradient by blood flow restriction. The mice were divided into five groups: PBS ($n = 5$), nAT-MSC ($n = 30$), dAT-MSC ($n = 30$), dAT-MSC-mock ($n = 5$), and dAT-MSC small hairpin RNA-targeted EGR-1 (shEGR-1) ($n = 6$). In each of the AT-MSC transplantation groups, cells were injected locally on the dorsal surface at four positions (5×10^5 cells/200 μL IMDM/mouse). Immunosuppression was induced by the intraperitoneal injection of cyclosporin A (20 mg/kg body weight; Wako) every 2 days. We previously demonstrated that the efficiency of wound healing of C57/BL6 mice with injection of cyclosporin A was not different from that of BALB/c nu/nu mice without the cyclosporin A treatment [25], therefore, we used C57/BL6 mice with the cyclosporin A treatment in this study. After 7 days, 200 μL of Bandeiraea simplicifolia-I (BS-I) Lectin-TRITC (0.1 mg/mL; Sigma-Aldrich) was injected into the tail vein, ~30 min before sacrifice. Images of the ischemic flap were captured. The flap tissue was embedded and sectioned for analysis.

Histological analysis

The tissue structure and vessel formation were stained using H&E counterstain and BS-I Lectin-TRITC, respectively. The inflammatory cells in the ischemic tissue were examined by immunohistochemical staining with PE-labeled anti-CD45 (30F11; BD Pharmingen). The relative value of vessel per area was based on the fluorescence intensity ratio per each field and measured by ImageJ software (NIH). A number of CD45 cells were counted in each field. The presented data were the average of 10 fields per data.

Statistical analysis

Student's *t*-test was used to determine the significance of differences between two experimental groups. The one-way analysis of variance, followed by Bonferroni post-hoc test (SPSS software; IBM Corp.), were used to determine statistical differences among three or four experimental groups. A P value <0.05 was considered to indicate statistical significance. All of the data are presented as the mean ± standard deviation.

Results

The differentiation potential and the expression of mesenchymal stem cell surface markers in nAT-MSCs and dAT-MSCs

AT-MSCs are known to possess the ability to differentiate into several types of mesenchymal cells and to express some mesenchymal stem cell markers [26–28]. To examine the differentiation potential of dAT-MSCs, we first cultured nAT-MSCs and dAT-MSCs under conditions that would induce differentiation into osteoblasts, adipocytes, and chondrocytes. Alizarin Red, Oil Red O, and Toluidine Blue staining were performed to examine calcification in osteoblasts, lipid accumulation in adipocytes, and cartilage proteoglycan synthesis in chondrocytes, respectively (Fig. 1A). Both nAT-MSCs and dAT-MSCs had the same potential to differentiate into osteocytes and chondrocytes (Fig. 1A, B). On the other hand, the differentiation ability toward adipocyte lineage was higher in dAT-MSC than that in nAT-MSC. Consistent with these observations, the expression levels of the two adipocyte-specific genes (PPARγ2 [29] and adiponectin [30]) were greater in dAT-MSCs than in nAT-MSCs, whereas the expression levels of the osteogenic genes (Runx2 [31] and ALP [32]) in dAT-MSCs and nAT-MSCs were comparable (Fig. 1C). A flow cytometric analysis revealed that the MSC-specific cell surface markers, except CD166/ALCAM were expressed at similar levels in both dAT-MSCs and nAT-MSCs (Fig. 1D). CD166/ALCAM expressed higher in dAT-MSCs compared with nAT-MSCs. It has been reported that CD166/ALCAM is a close structural and functional homolog of RAGE [33], and RAGE-mediated regulation of adiposity and inflammation associated with T2DM and diabetic vascular complications [34]. Collectively, these findings demonstrate that of these two types of AT-MSCs, dAT-MSCs possess a greater potential to differentiate into adipocytes; the other phenotypes were indistinguishable from nAT-MSCs.

The ability to improve wound healing is impaired in dAT-MSCs in the mouse skin flap model

We next examined the proliferation activity of nAT-MSCs and dAT-MSCs. In the log phase, the average doubling time in nAT-MSCs and dAT-MSCs was similar under both normoxic and hypoxic conditions (Fig. 2A). As expected, both types of AT-MSCs proliferated faster under hypoxic conditions. On day 7 of culture, when the cells reached confluence, the dAT-MSCs that were cultured under hypoxic conditions appeared to be difficult to dissociate into single cell suspensions by trypsinization. Even with an extended treatment time with a higher concentration of trypsin/EDTA, the number of countable dAT-MSCs was much lower due to cell aggregation (Fig. 2B). The increased cell aggregation and adhesion of the dAT-MSCs only appeared under hypoxic conditions. We hypothesized that the increased aggregation and adhesion of dAT-MSCs might affect their regenerative activity in ischemic tissue in vivo. To test this, the wound healing activity of AT-MSCs was

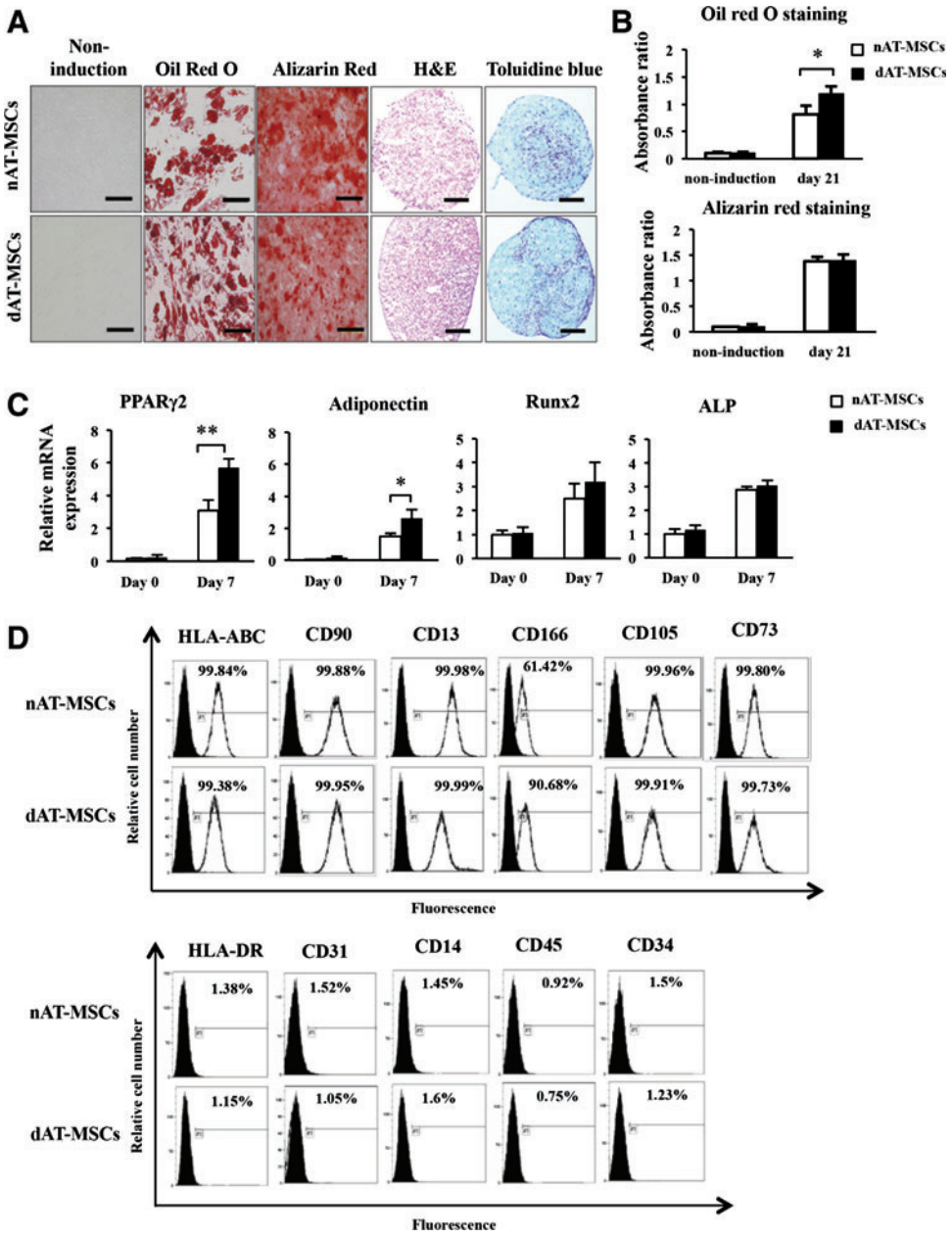

FIG. 1. The differentiation potential and expression of mesenchymal stem cell surface makers in non-diabetic adipose tissue-derived mesenchymal stem cells (nAT-MSCs) and diabetic adipose tissue-derived mesenchymal stem cells (dAT-MSCs). **(A)** Differentiated cells were recognized on day 21 using Alizarin Red staining, which indicated the calcification of the surface of osteoblasts (*red*). Oil Red O staining indicated the lipid accumulation of adipocytes (*red*); Hematoxylin and Eosin (H&E) staining was performed as a control. Toluidine Blue staining indicated cartilage proteoglycan and glycosaminoglycan (*purple*). Scale bar: 200 μm. **(B)** Absorbance was measured at 482 and 490 nm for Alizarin Red and Oil Red O staining, respectively. In the Oil Red O staining of dAT-MSCs, absorbance was significantly higher than that in nAT-MSCs. **(C)** The expression of differentiated master genes was examined by a quantitative reverse transcription polymerase chain reaction (qRT-PCR) and normalized to β-actin on days 0 and 7 of osteogenic and adipogenic induction. The level of osteogenic differentiation in dAT-MSCs was similar to that in nAT-MSCs, whereas the level of adipogenic differentiation in dAT-MSCs was significantly higher than that in nAT-MSCs. The expression levels of Runx2, ALP, PPARγ2, and adiponectin were determined by a qRT-PCR. **(D)** nAT-MSCs and dAT-MSCs were analyzed and sorted by a FACS Vantage SE to determine the expressions of HLA-ABC, CD90, CD13, CD166, CD105, CD73, HLA-DR, CD31, CD14, CD45, and CD34 (*line peaks*) in comparison to isotype controls (*black peaks*). The *white* and *black bars* indicate nAT-MSCs and dAT-MSCs, respectively. Data represent the average of three independent experiments (mean ± SD); $*P < 0.05$; $**P < 0.01$. SD, standard deviation. Color images available online at www.liebertpub.com/scd

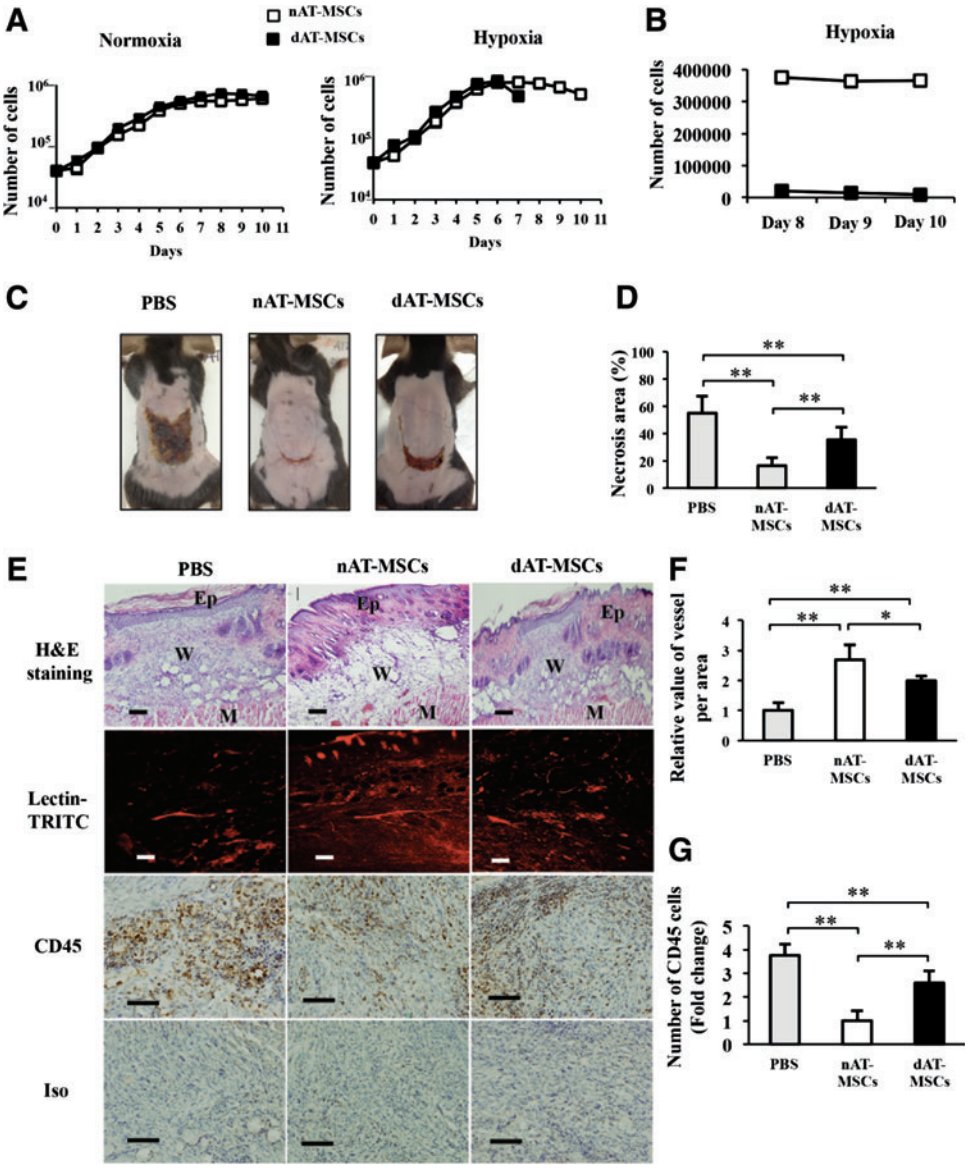

FIG. 2. The ability to improve wound healing is impaired in dAT-MSCs in the mouse skin flap model. **(A)** The number of cells was counted every 24 h using Trypan Blue exclusion over 10 days under normoxic (20% O_2) or hypoxic (5% O_2) conditions. Abnormal cell adhesion was observed in dAT-MSCs under hypoxic conditions on day 7. The precise number of cells could not be counted because the cells adhered together too tightly. The average doubling time was 32.5 ± 2 h under normoxic conditions and 28.5 ± 2 h under hypoxic conditions ($P < 0.01$). **(B)** The number of dAT-MSCs was counted after abnormal cell adhesion and compared with the number of nAT-MSCs on days 8, 9, and 10. **(C)** Images of the necrotic areas of mice injected with PBS, nAT-MSCs, and dAT-MSCs were captured on day 7 after injection. **(D)** The percentage of the necrotic area was calculated based on the necrotic area per wound area in mice that were injected with PBS ($n = 5$), nAT-MSCs ($n = 30$), and dAT-MSCs ($n = 30$). **(E)** The embedded sections were examined by H&E staining for tissue structure, which revealed the epidermis, wound, and muscle in each wound site; BS-I Lectin-TRITC was injected into the tail vein to observe the vessel formation (*red*) with fluorescence intensity; and the CD45 immunohistochemical staining of inflammatory cells (*brown*). **(F)** The fluorescence intensity was measured using the ImageJ software program to evaluate the number of vessels in each area ($n = 20$). **(G)** The CD45-positive cells were counted and expressed relative to the number nAT-MSCs ($n = 10$). Data represent the average of three independent experiments (mean ± SD); $*P < 0.05$; $**P < 0.01$. Scale bars: 100 μm; BS-I, Bandeiraea simplicifolia-I; Ep, epidermis; M, muscle; W, wound. Color images available online at www.liebertpub.com/scd

examined using mice with an ischemic flap. Although the injection of both AT-MSCs improved the recovery from injury at 1 week after surgery, the necrotic surface area was larger in the dAT-MSC-injected mice than in the nAT-MSC-injected mice (Fig. 2C, D). The H&E staining of the ischemic flap revealed a hypertrophic epidermis, which resembled normal wound healing, in the nAT-MSC-injected mice. In contrast, the hypertrophy of the epidermis was less evident in the dAT-MSC-injected mice (Fig. 2E). The improved wound healing of the nAT-MSC-injected mice was also shown by Lectin-TRITC staining, which shows the active neovascularization. Notably, the formation of

neovascularization was less prominent in the flap in the dAT-MSC-injected mice (Fig. 2E, F). At 1 week after surgery, the flap of the untreated mice showed significant CD45-positive cell infiltration, suggesting that the inflammation that occurred in response to tissue injury was prolonged (Fig. 2E, G). In contrast, the number of CD45-positive cells in the flap of the nAT-MSC-injected mice was much lower than that in the untreated mice (Fig. 2E, G). A greater number of CD45-positive cells were observed in the flap of the dAT-MSC-injected mice than in the nAT-MSC-injected mice (Fig. 2E, G). Taken together, these findings indicate the impaired ability of dAT-MSCs to improve wound healing in the ischemic flap in our mouse model of ischemia.

The expression of EGR-1 is increased in dAT-MSCs

To explore the molecular basis for the impaired wound healing effects of dAT-MSCs, we focused on EGR-1, a zinc finger transcription factor, since the overexpression of this molecule in adipocytes has been reported to promote insulin resistance in T2DM patients [35]. Indeed, EGR-1 protein was more abundant in dAT-MSCs than in nAT-MSCs under both normoxic and hypoxic conditions (Fig. 3A). A quantitative RT-PCR revealed that the mRNA level of EGR-1 was significantly greater in dAT-MSCs than in nAT-MSCs, indicating that EGR-1 was upregulated at the transcriptional level (Fig. 3A). Although the expression of

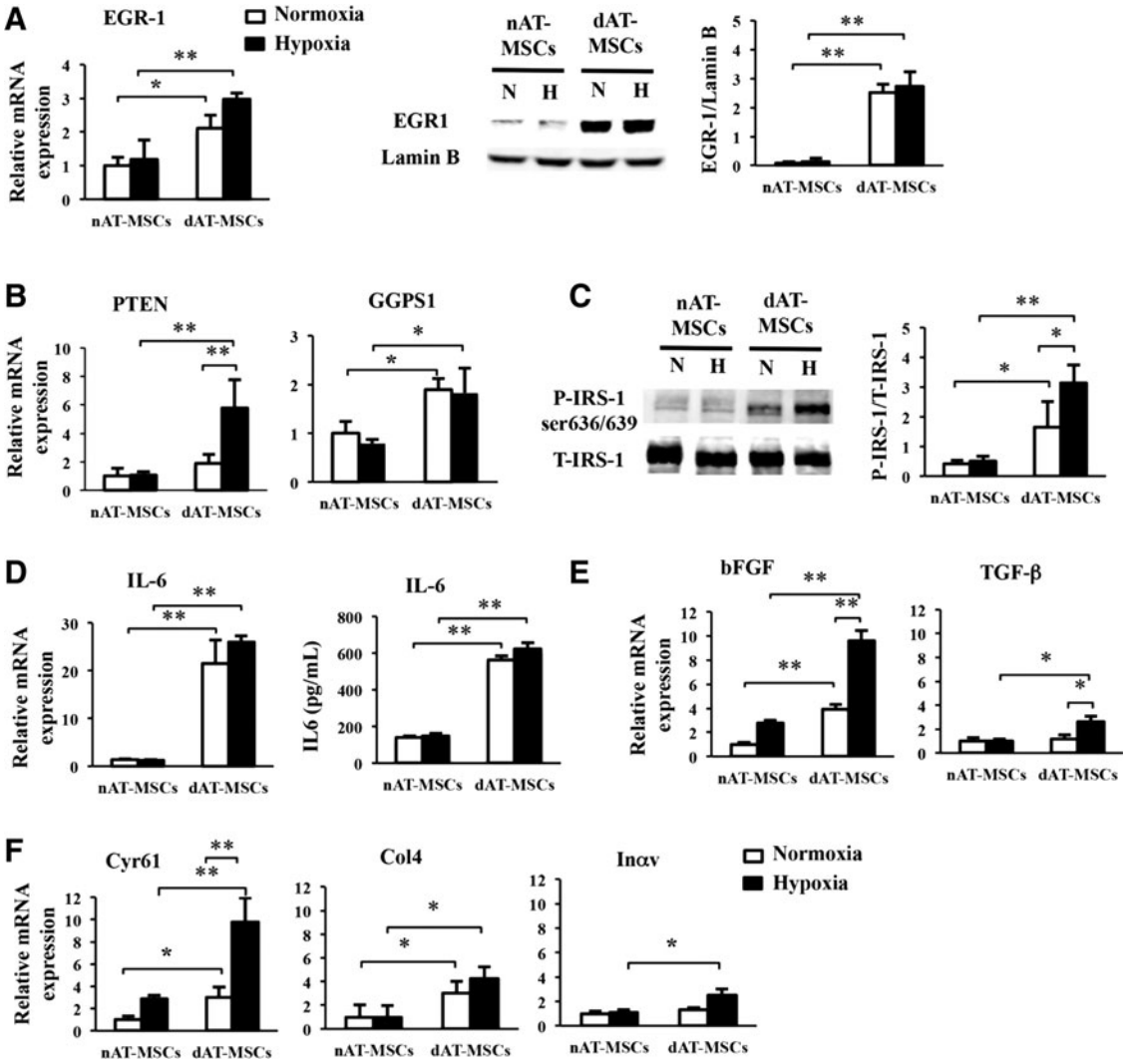

FIG. 3. The expression of EGR-1 is increased in dAT-MSCs. **(A)** nAT-MSCs and dAT-MSCs were cultured under normoxic (20% O_2) or hypoxic (5% O_2) conditions. The mRNA and protein levels of transcription factor EGR-1 were examined by a qRT-PCR and an immunoblot analysis, respectively, normalized to β-actin and Lamin B. **(B)** *PTEN* and *GGPS1* expression was determined by a qRT-PCR and normalized to β-actin. **(C)** Insulin (1,000 nM) was added to the culture medium for 60 min to stimulate the phosphorylation of IRS-1 (P-IRS-1). P-IRS-1 at serine 636/639 and total IRS-1 (T-IRS-1) were analyzed by immunoblotting. **(D)** The mRNA expression level of interleukin-6 (IL-6) was assessed by a qRT-PCR and normalized to β-actin, and the quantitative protein concentration of IL-6 present in cell culture supernatants was measured by the IL-6 High Sensitivity Human ELISA Kit (D6050; R&D systems). **(E, F)** The mRNA expression levels were assessed by a qRT-PCR and normalized to β-actin to determine the expression of bFGF and TGF-β **(E)**, Cyr61, Col4, and Inαv **(F)**. *White* and *black bars* indicate normoxic and hypoxic conditions, respectively. Data represent the averages of three independent experiments (mean ± SD); $*P < 0.05$, $**P < 0.01$. EGR-1, early growth response factor-1; ELISA, enzyme-linked immunosorbent assay; H, hypoxia; N, normoxia.

EGR-1 is known to be rapidly and transiently induced by stress signals, including hypoxia, it is noteworthy that EGR-1 was highly expressed in dAT-MSCs, even under normoxic conditions. Consistent with these observations, the mRNA levels of the two target molecules of EGR-1 in adipocytes, PTEN [36] and GGPPS [14], were higher in dAT-MSCs than in nAT-MSCs. Interestingly, although the level of EGR-1 protein was comparable under normoxic and hypoxic conditions, hypoxia induced the expression of *PTEN*, but not *GGPS1* (the gene encoding *GGPPS*) (Fig. 3B).

A previous study reported that the phosphorylation of insulin receptor substrate-1 (IRS-1) at Ser636 was increased in skeletal muscle cells from T2DM patients due to an increase in basal MAPK activity [37]. Since EGR-1 has been shown to augment Erk/MAPK signaling through the upregulation of GGPPS [15], we examined whether the phosphorylation of Ser636/639 by IRS-1 was increased in dAT-MSCs by western blot analysis (Fig. 3C). In the absence of insulin, we did not observe any phosphorylation of Ser636/639 of IRS-1 (data not shown). In contrast, in the presence of insulin, the phosphorylation of Ser636/639 of IRS-1 was observed in dAT-MSCs under the normoxic conditions; this phosphorylation was further increased under hypoxic conditions (in place of the phosphorylation of IRS-1 on tyrosine sites [38]) (Fig. 3C).

Aside from its role in insulin signaling, EGR-1 has been shown to play multiple roles in the regulation of the inflammatory response [39], fibrogenesis [40], and cell adhesion [39]. Since our findings showed that the wound healing effects in the mouse skin flap model were impaired in dAT-MSCs, we examined the mRNA level of IL-6 in dAT-MSCs, and found that it was more than 25-fold higher than that in nAT-MSCs under both normoxic and hypoxic conditions, and the protein level was 4-fold higher in dAT-MSCs compared with nAT-MSCs measured by ELISA (Fig. 3D). In addition, the mRNA levels of the cytokines and adhesion molecules that are known to be regulated by EGR-1 [39,41] was examined using a quantitative RT-PCR. We found that the expression levels of EGR-1 target cytokines (bFGF and TGF-β) were significantly higher in dAT-MSCs compared with nAT-MSCs under hypoxic conditions (Fig. 3E). Although the mRNA level of bFGF was observed to be increased in dAT-MSCs in comparison to nAT-MSCs, irrespective of oxygen tension, the upregulation of TGF-β in dAT-MSCs was only observed under hypoxic conditions (Fig. 3E). Among the known EGR-1 target genes that encode cell adhesion molecules, Cyr61 and Col4 were more highly expressed in dAT-MSCs than in nAT-MSCs, irrespective of oxygen tension, whereas the increased expression of Inαv was only observed under hypoxic conditions (Fig. 3F). Collectively, these data suggest an important role of EGR-1 in regulating many target genes that respond to insulin resistance, cell adhesion, and inflammation that may associate with the impaired wound healing activity of dAT-MSCs in vivo.

Activated ERK1/2 signaling is the major upstream signal of EGR-1 activation in dAT-MSCs

It has been shown that EGR-1 expression is induced by various stress signals, including tissue injury, oxidative stress, and hypoxia [42]. In vascular smooth muscle cells, EGR-1 expression is induced by hemin through the activation of ERK1/2 [43]. To determine the upstream signaling that is involved in the activation of EGR-1 in dAT-MSCs, we examined the effect of PD98059, an inhibitor of MAPK/ERK kinase, on the EGR-1 protein levels in AT-MSCs. The level of ERK1/2 phosphorylation in both types of AT-MSCs was clearly reduced by PD98059 treatment, whereas the treatment did not affect the phosphorylation of AKT at serine 473 (Fig. 4A). EGR-1 expression was almost completely repressed by PD98059 in both types of AT-MSCs under normoxic conditions (Fig. 4B). Interestingly, however, the persistent expression of EGR-1 was detected in the PD98059-treated dAT-MSCs under hypoxic conditions, suggesting that an additional upstream signal is involved in the EGR-1 induction in dAT-MSCs under hypoxic conditions (Fig. 4B). Although EGR-1 expression is known to be induced by hypoxia, the direct effect of HIF-1α on EGR-1 gene transcription is controversial, since hypoxia-induced EGR-1 expression is retained in hepatoma cells which lack HIF-1β (a heterodimeric partner of HIF-1α) [13]. In support of this hypothesis, the induction of HIF-1α was similarly observed in both types of AT-MSCs, despite EGR-1 expression being constitutively activated in dAT-MSCs (Fig. 4C). Interestingly, a ChIP assay revealed that, under hypoxic conditions, HIF-1α binds directly to a putative HRE within the EGR-1 promoter in dAT-MSCs, but not in nAT-MSCs (Fig. 4D). These data indicate that the increased EGR-1 expression that is observed in dAT-MSCs under hypoxic conditions is mediated by at least two distinct mechanisms: ERK1/2 signaling activation and direct transcriptional activation by HIF-1α. To evaluate the relative contribution of the ERK1/2 pathway in dAT-MSCs on the expression of the EGR-1 target genes, the effect of PD98059 on the expression of the EGR-1 target genes was examined by a quantitative RT-PCR (Fig. 4E, F). In the presence of PD98059, the mRNA levels of all of the cytokines and adhesion molecules that were examined were reduced in dAT-MSCs to levels that were comparable to those in nAT-MSCs (Fig. 4E, F). As a result of the remarkable changes of IL6 and Cyr61 in mRNA levels, we analyzed these two proteins by western blot and ELISA (Fig. 4G, H). Our data confirmed that the protein level of IL6 and Cyr61 were remarkably increased in dAT-MSCs compared with nAT-MSCs. Consistent with the result in mRNA expression, the expressions of IL6 and Cyr61 were significantly decreased in dAT-MSCs the presence of the inhibitor (Fig. 4G, H). Thus, these data suggest that the ERK1/2 pathway is the major upstream signal for the expression of EGR-1 in dAT-MSCs. On the other hand, the effect of HIF-1α on EGR-1 expression is minor, but is specifically observed in AT-MSCs under diabetic conditions.

The constitutive activation of EGR-1 is responsible for the impaired wound repair activity of dAT-MSCs

Our findings showed that dAT-MSCs were less effective for improving wound repair in the ischemic flap and that EGR-1 expression was constitutively activated in dAT-MSCs. To provide direct evidence of the involvement of EGR-1 in the impaired wound healing activity of dAT-MSCs, EGR-1 expression was knocked down by shRNA. As shown in Fig. 5A, EGR-1 expression was reduced by shRNA in dAT-MSCs at both the mRNA and the protein

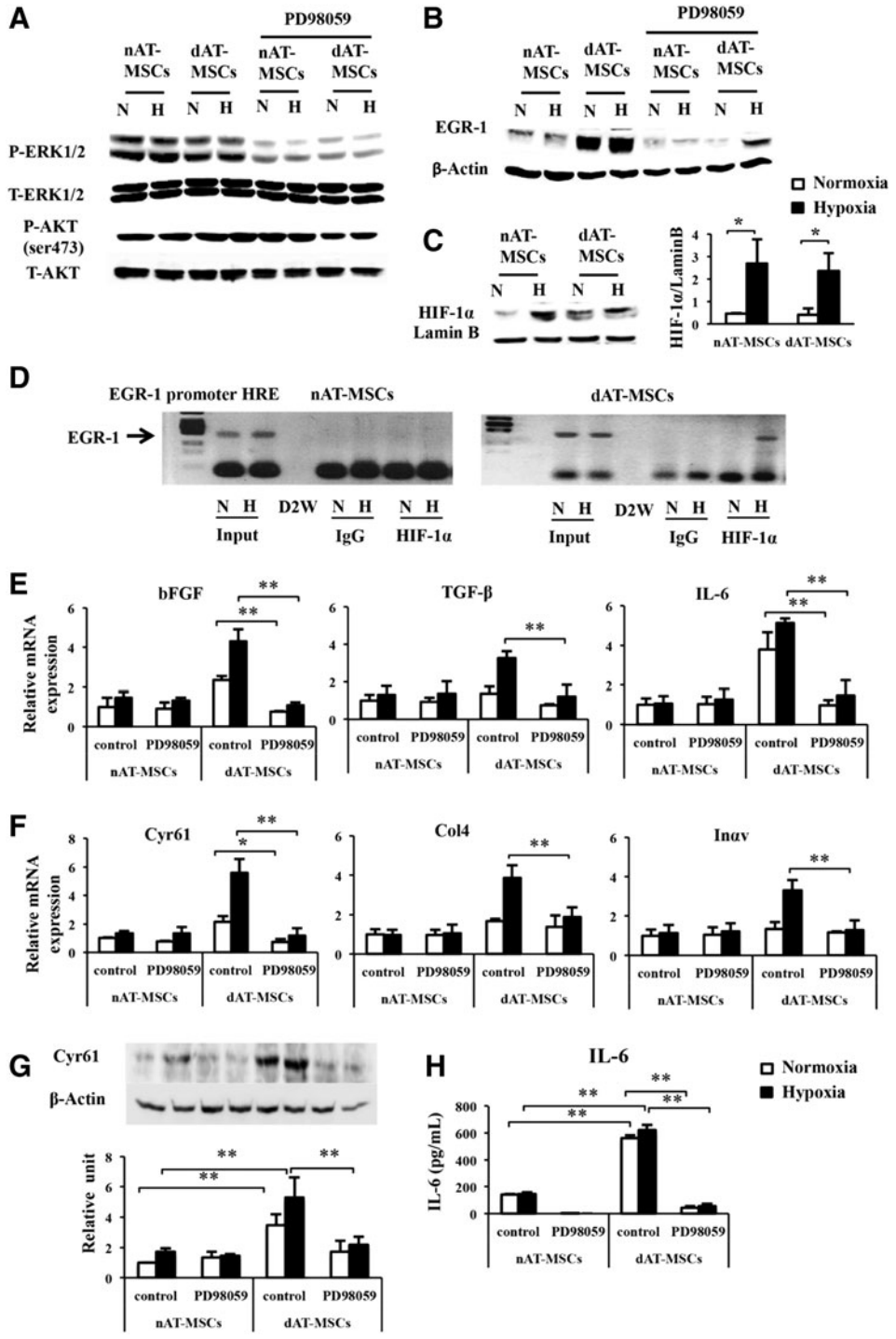

FIG. 4. Activated ERK1/2 signaling is the major upstream signal of EGR-1 activation in dAT-MSCs. PD98059 (50 μM) was added to nAT-MSC and dAT-MSC cultures for 60 min that were maintained under normoxic (20% O_2) or hypoxic (5% O_2) conditions. Whole cell proteins were prepared for an immunoblot analysis. **(A)** The phosphorylation of ERK1/2 and total ERK1/2 (T-ERK1/2), the phosphorylation of AKT at serine 473, and total AKT (T-AKT) were examined in treated and untreated cells under normoxic and hypoxic conditions. **(B)** The expression levels of EGR-1 and internal control β-Actin were also assessed by immunoblotting in treated and untreated cells under nomoxic and hypoxic conditions. **(C)** HIF-1α expression was assessed in nAT-MSCs and dAT-MSCs under normoxic and hypoxic conditions by an immunoblot analysis and normalized to Lamin B. **(D)** A chromatin immunoprecipitation (ChIP) assay was performed for the EGR-1 promoter HRE using an anti-HIF-1α antibody under normoxic (20% O_2) and hypoxic (5% O_2, 4 days) conditions. Input samples (1/10 input) were used as an internal control; IgG was used as a negative control. The binding of HIF-1α to the EGR-1 promoter was specified in dAT-MSCs under hypoxic conditions. **(E, F)** The mRNA expression levels of the EGR-1 target genes were examined by a qRT-PCR and normalized to β-Actin, including bFGF, TGF-β, and IL-6 **(E)**, and Cyr61, Col4, and Inαv **(F)**. **(G)** The protein levels of Cyr61 was examined by immunoblot analysis, and normalized to β-Actin. **(H)** The quantitative protein concentration of IL-6 present in cell culture supernatants was measured by ELISA. The *white* and *black bars* indicate normoxic and hypoxic conditions, respectively. Controls representative of nontreated cells. Data shown are the averages of three independent experiments (mean ± SD). $*P < 0.05$; $**P < 0.01$. ERK, extracellular signal-regulated kinase; H, hypoxia; HIF-1α, hypoxia-inducible factor-1α; N, normoxia.

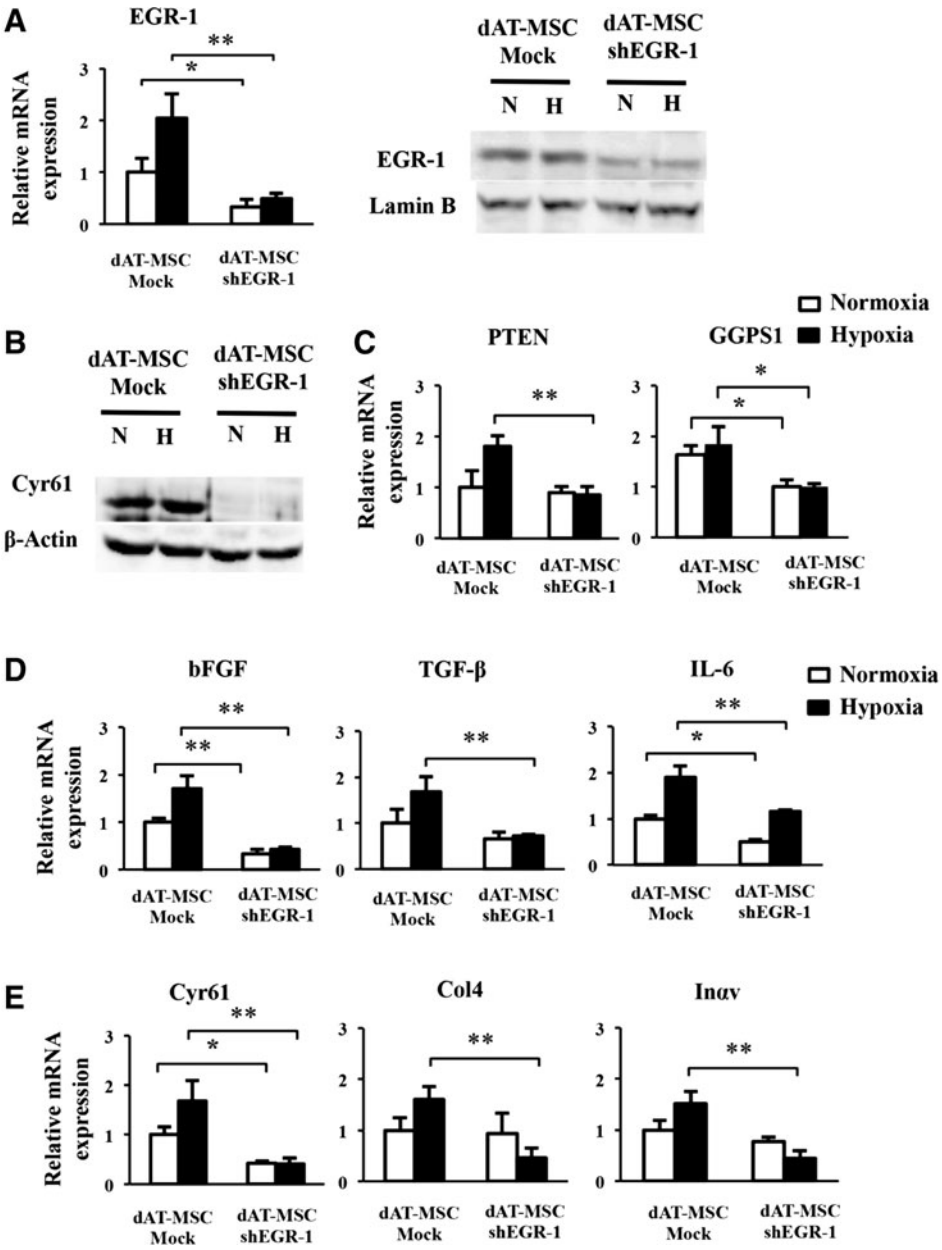

FIG. 5. The constitutive activation of EGR-1 is responsible for the impaired wound repair activity of dAT-MSCs. **(A)** dAT-MSCs were transfected with shRNA lentiviral transduction particles targeting EGR-1 (dAT-MSC-shEGR-1). The control cells were transfected with lentiviral control (dAT-MSC-Mock). After puromycin selection, the cells were cultured under normoxic (20% O_2) and hypoxic conditions (5% O_2) for 4 days. The mRNA and protein levels of EGR-1 were examined by a qRT-PCR and an immunoblot analysis, respectively. **(B)** The protein levels of Cyr61 and the internal control β-Actin were assessed by immunoblot analysis. **(C–E)** The mRNA expression levels of the EGR-1 target genes were assessed by a qPCR and normalized to β-Actin, including *PTEN* and *GGPS1* **(C)**; bFGF, TGF-β, and IL-6 **(D)**; Cyr61, Col4, and Inαv **(E)**. The *white* and *black bars* indicate normoxic and hypoxic conditions, respectively. Data represent the averages of three independent experiments (mean ± SD); $*P < 0.05$, $**P < 0.01$.H, hypoxia; N, normoxia; shEGR-1, small hairpin RNA targeted EGR-1.

level (Fig. 5A). In accordance with the reduction in EGR-1, the expression of Cyr61 at the protein level was abolished in the knockdown EGR-1-dAT-MSCs under both normoxic and hypoxic conditions (Fig. 5B). In addition, the expression levels of *PTEN* and *GGPS1*, three cytokines (bFGF, TGF-β, and IL-6), and three adhesion molecules (Cyr61, Col4, and Inαv) were significantly decreased under hypoxic conditions (Fig. 5C–E). In accordance with the result in Fig. 4E and F, the gene expression levels of TGF-β, Col4, and Inαv were not affected by PD98059 in dAT-MSCs under normoxic conditions (Fig. 4E, F). The mRNA level of *PTEN*, TGF-β, Col4, and Inαv was not significantly reduced by shEGR-1 under normoxic conditions in dAT-MSCs, whereas the expression levels of the other genes were comparable in both types of AT-MSCs under normoxic conditions (Fig. 5C–E). These data suggest that the role of EGR-1 in the regulation of these genes was restricted under normoxic conditions.

The reduced expression of EGR-1 in dAT-MSCs promotes wound repair activity

To examine whether the repression of EGR-1 by shRNA restored the ability to improve wound healing in dAT-MSCs, the wound healing activity of EGR-1-deficient dAT-MSCs was examined using the mouse skin flap model (Fig. 6A). We found that the knockdown of EGR-1 in dAT-MSCs significantly reduced the necrotic surface area of the ischemic flap. The H&E staining of the wound section showed that the epidermis of mice injected with EGR-1-deficient dAT-MSCs was thicker than that in mice that were injected with dAT-MSCs (Fig. 6B). Moreover, neovascularization was significantly increased, whereas the infiltration of CD45-positive cells was reduced in the EGR-1-deficient dAT-MSCs in comparison to the controls (Fig. 6B–D). Collectively, these data suggest that the constitutive activation of EGR-1 is responsible for the

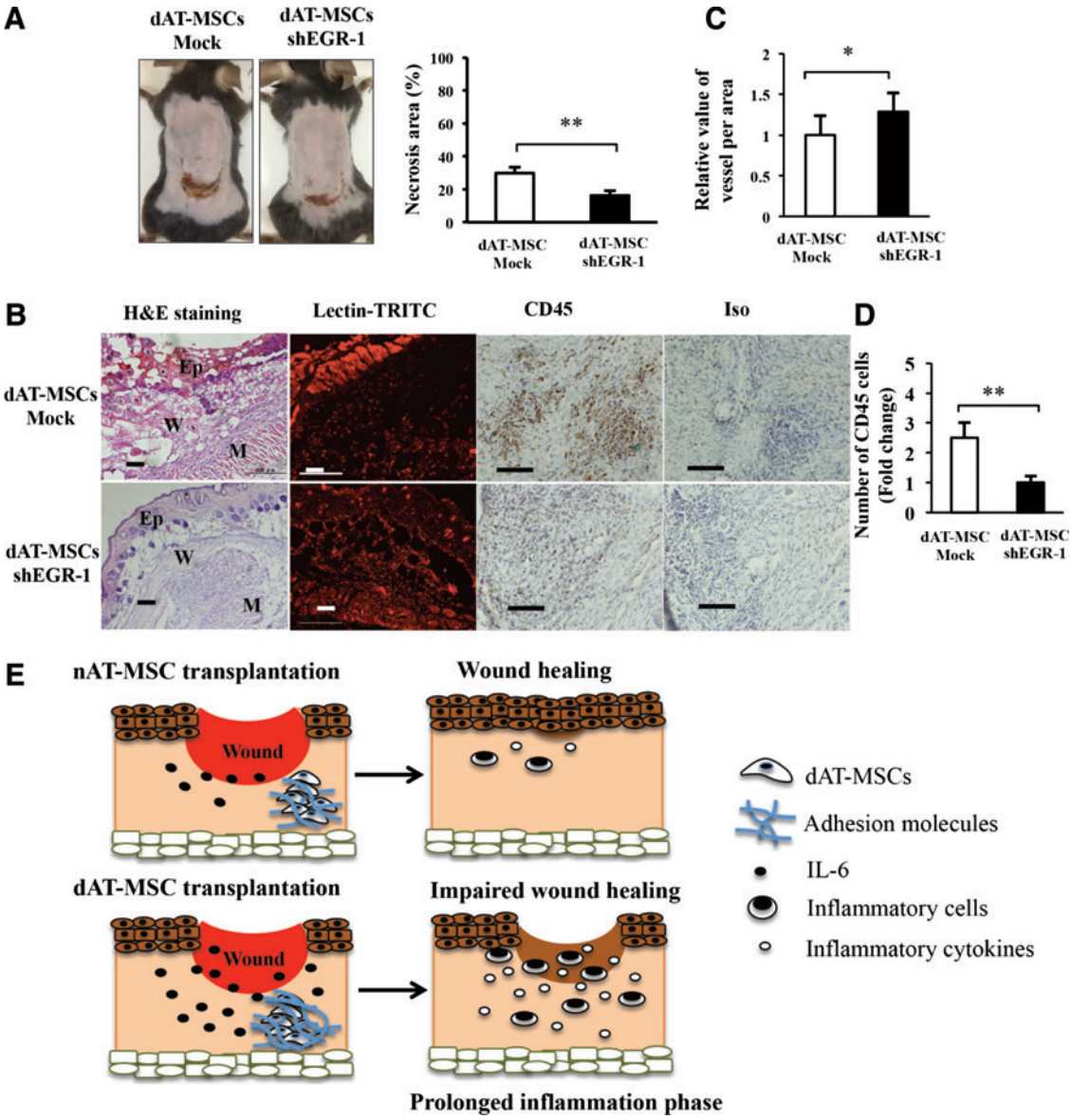

FIG. 6. The reduced expression of EGR-1 in dAT-MSCs promotes wound repair activity. **(A)** Images of necrotic areas in mice that were injected dAT-MSC-mock and dAT-MSC-shEGR-1 were captured at day 7 after transplantation. The percentage of the necrotic area was calculated based on the area of necrotic tissue in relation to the wound area of mice injected with dAT-MSC-mock ($n=5$) and dAT-MSC-shEGR-1 ($n=6$). The knockdown of EGR-1 significantly increased the rate of wound healing in comparison to the control group. **(B)** The embedded sections were examined by H&E staining for tissue structure, which revealed the epidermis, wound, and muscle in each wound site; BI Lectin-TRITC staining was used to reveal the vessel formation (*red*); CD45 immunohistochemistry staining was performed to identify the inflammatory cells (*brown*). **(C)** The activity of vessel formation in each area was measured based on fluorescence intensity using the ImageJ software program ($n=20$). **(D)** The number of CD45-positive cells were counted relative to the number of dAT-MSC-mock cells ($n=10$). **(E)** A schematic illustration of wound healing process with nAT-MSC or dAT-MSC transplantation. The wound healing ability of dAT-MSCs was impaired due to adhesion molecules and excessive IL-6. This impairment might lead to a prolonged inflammation phase and delayed wound healing in comparison to the normal wound healing process with nAT-MSC transplantation. Data represent the average results from independent experiments (mean ± SD). $^{*}P<0.05$; $^{**}P<0.01$. Scale bars: 100 μm; Ep, epidermis; M, muscle; W, wound. Color images available online at www.liebertpub.com/scd

impaired wound repairing activity of the AT-MSCs derived from T2DM patients.

Discussion

In the present study, we found that EGR-1 is constitutively activated in AT-MSCs derived from T2DM patients. We focused on this molecule because its overexpression in adipocytes plays a central role in insulin resistance in T2DM patients [14,15]. The overexpression of EGR-1 leads to the activation of two critical target genes (*PTEN* and *GGPS1*) in adipocytes. While GGPPS activates MAPK/ERK1/2 signaling, PTEN impairs PI3K/Akt signaling, thereby reducing signals from insulin receptors in T2DM adipocytes [14,15].

Our data showed the increased expression of *PTEN* and *GGPS1* and the phosphorylation of IRS-1 at serine 636/639 in dAT-MSCs, suggesting an early manifestation of insulin resistance at the stem cell level under diabetic conditions.

Our data showed that dAT-MSCs appeared to aggregate exclusively under hypoxic conditions in vitro, and that these cells were less effective for improving wound healing in the mouse skin flap model. The repression of EGR-1 by shRNA restored the ability of dAT-MSCs to improve wound healing, suggesting that EGR-1 is responsible for the impaired wound repair ability of dAT-MSCs (Fig. 6). Notably, the reduction of EGR-1 in dAT-MSCs significantly improved neovascularization at the wound site on the ischemic flap (Fig. 6C). Macro/microangiopathy in T2DM patients is characterized by the increased expression of a variety of growth factors and adhesion molecules [2,16]. For instance, bFGF and TGF-β are known to increase vascular permeability and coagulation, which leads to blood flow abnormalities in patients with diabetic angiopathy [2,44]. Cyr61, Col4, and Inαv are the markers of microangiopathy in diabetic patients [45–47]. In agreement with previous reports, our results showed the upregulation of these growth factors and adhesion molecules in dAT-MSCs at the mRNA level (Fig. 3). Importantly, Cyr61 is an extracellular matrix protein and plays an important role as an angiogenic mediator. It has been reported that Cyr61 participates in the pathogenesis of proliferative diabetic retinopathy and rheumatoid arthritis [45,48]. In this study, the mRNA and protein levels of Cyr61 were significantly decreased in both PD98059-treated dAT-MSCs and in EGR-1 knockdown dAT-MSCs (Figs. 4F and 5E). In addition, the expression of Cyr61 at the protein level was diminished in dAT-MSCs treated with inhibitor or shEGR-1 (Figs. 4G and 5B).

IL-6 has been shown to play critical roles in T2DM, obesity, and cardiovascular diseases [15,49,50]. The circulating levels of plasma IL-6 are increased in T2DM patients who are treated with insulin [51]. Excessive amounts of IL-6 have been shown to prolong the inflammatory response in injuries and to delay the wound healing process [52,53]. In fact, the expression of IL-6 in dAT-MSCs was 25-fold higher at the mRNA level and 4-fold increase at the protein level compared to nAT-MSCs (Fig. 3E). The expression of IL-6 was downregulated in the presence of PD98059 at the mRNA (Fig. 4E) and protein levels (Fig. 4H). Thus, it is likely that IL-6 plays a key role in the impairment of the wound healing ability of dAT-MSCs.

Further studies are required to determine the precise roles of the individual cytokines and adhesion molecules that are highly expressed in dAT-MSCs under normal or diabetic conditions in vivo (*db/db* mice).

The increased expression of EGR-1 has also been reported in patients with scleroderma, an autoimmune disease that affects collagen [39]. The induction of EGR-1 by TGF-β plays an important role in the promotion of fibrosis in the fibroblasts of scleroderma patients [54]. Interestingly, in EGR-1 null mice, the impaired healing of cutaneous wounds and fibroblast-specific EGR-1 overexpression under the control of the Col1a2 promoter resulted in the robust healing of incisional wounds [38]. In contrast, the aberrant and persistent expression of EGR-1 in peripheral tissue promoted scleroderma and pulmonary fibrosis in a murine model [55,56]. Taken together with our present data, these results suggest that EGR-1 plays a dual role in wound healing, which is dependent on the cellular context. Given that fibroblasts are descendants of MSCs, the biological function of EGR-1 might change with cellular differentiation. Thus, the rigorous regulation of EGR-1 expression would be important for the appropriate control of wound healing.

Although several studies have suggested EGR-1 to be a hypoxia-inducible gene, the elevated expression of EGR-1 in dAT-MSCs was constitutively observed under both normoxic and hypoxic conditions (Fig. 3A). Since EGR-1 expression was clearly diminished by PD98059, an inhibitor of MAPK/ERK kinase ERK1/2 (Fig. 4B), MAPK signaling is likely to be the major upstream regulator of EGR-1 in dAT-MSCs. In fact, phosphorylated ERK activates ELK-1 binding to serum response elements in EGR-1 promoter [57], indicating that MAPK signaling pathway promotes mutual activation of EGR-1 expression in both AT-MSCs. Of note, the residual expression of EGR-1 was found in dAT-MSCs under hypoxic conditions (Fig. 4B), suggesting the existence of an additional pathway of EGR-1 regulation in dAT-MSCs under hypoxic conditions. We performed a ChIP assay and found that HIF-1α bound directly to the EGR-1 promoter in dAT-MSCs, suggesting that EGR-1 expression is regulated by both MAPK signaling and HIF-1α in dAT-MSCs. This regulatory pathway of EGR-1 by HIF-1α is relatively minor; however, under certain pathological conditions, it might play a specific role in T2DM patients. Interestingly, although the EGR-1 protein levels were similar under normoxic and hypoxic conditions, EGR-1 shRNA treatment resulted in the reduction of a group of genes (TGF-β, Col4, and Inαv) under hypoxic, but not normoxic conditions (Fig. 5C, D). Consistently, PD98059 only affected the expression of these genes under hypoxic conditions (Fig. 4). These results suggest that the expression of these genes is only regulated by EGR-1 under hypoxic conditions. The molecular mechanism underlying the functional differences of EGR-1 under normoxic and hypoxic conditions remains to be elucidated.

In conclusion, the present study demonstrates that the expression of EGR-1 was upregulated in dAT-MSCs through two different pathways. The main regulatory pathway is the MAPK/ERK pathway, which is independent of oxygen tension. The other regulatory pathway is mediated by HIF-1α through the direct transcriptional activation at the promoter region of the *EGR1* gene. The latter is observed under hypoxic conditions in dAT-MSCs, but not in nAT-MSCs. Our data demonstrate that a high level of EGR-1 is responsible for the impaired wound healing effect of dAT-MSCs. Thus, the control of EGR-1 expression by the manipulation of the upstream MAPK/ERK signaling and HIF factors could be a new therapeutic target for stem cell therapy in T2DM patients with chronic wounds and tissue ischemia.

Acknowledgments

The authors thank the Japanese Ministry of Education, Culture, Sports, Science & Technology (MEXT) and Mitsubishi Corporation's Japan Educational Exchanges and Services (JEES) for their support.

Author Disclosure Statement

No competing financial interests exist.

References

1. Donath MY and SE Shoelson. (2011). Type 2 diabetes as an inflammatory disease. Nat Rev Immunol 11:98–107.
2. Brownlee M. (2001). Biochemistry and molecular cell biology of diabetic complications. Nature 414:813–820.
3. Mavridis G, E Souliou, E Diza, G Symeonidis, F Pastore, AM Vassiliou and D Karamitsos. (2008). Inflammatory cytokines in insulin-treated patients with type 2 diabetes. Nutr Metab Cardiovasc Dis 18:471–476.
4. Knudsen SH and BK Pedersen. (2015). Targeting inflammation through a physical active lifestyle and pharmaceuticals for the treatment of type 2 diabetes. Curr Diab Rep 15:82.
5. Barnett AH, B Charbonnel, RG Moses and S Kalra. (2015). Dipeptidyl peptidase-4 inhibitors in triple oral therapy regimens in patients with type 2 diabetes mellitus. Curr Med Res Opin 11:1–13.
6. Singh K, NK Agrawal, SK Gupta, G Mohan, S Chaturvedi and K Singh. (2015). Increased expression of endosomal members of toll-like receptor family abrogates wound healing in patients with type 2 diabetes mellitus. Int Wound J 14:12411.
7. Gallagher KA, A Joshi, WF Carson, M Schaller, R Allen, S Mukerjee, N Kittan, EL Feldman, PK Henke, et al. (2015). Epigenetic changes in bone marrow progenitor cells influence the inflammatory phenotype and alter wound healing in type 2 diabetes. Diabetes 64:1420–1430.
8. Bekker-Mendez C, RM Guzman-Aguilar, MA Hernandez-Cueto, S Huerta-Yepez, RA Jarillo-Luna, E Gonzalez-Veyrand and CR Gonzalez-Bonilla. (2012). TUNEL-positive cells in the surgical border of an amputation due to infected diabetic foot. Mol Med Rep 5:363–372.
9. Greer SN, JL Metcalf, Y Wang and M Ohh. (2012). The updated biology of hypoxia-inducible factor. EMBO J 31: 2448–2460.
10. Semenza Gregg L. Hypoxia-inducible factors in physiology and medicine. Cell 148:399–408.
11. Girgis CM, K Cheng, CH Scott and JE Gunton. (2012). Novel links between HIFs, type 2 diabetes, and metabolic syndrome. Trends Endocrinol Metab 23:372–380.
12. Yan SF, N Mackman, W Kisiel, DM Stern and DJ Pinsky. (1999). Hypoxia/Hypoxemia-Induced activation of the procoagulant pathways and the pathogenesis of ischemia-associated thrombosis. Arterioscler Thromb Vasc Biol 19: 2029–2035.
13. Yan SF, J Lu, YS Zou, J Soh-Won, DM Cohen, PM Buttrick, DR Cooper, SF Steinberg, N Mackman, DJ Pinsky and DM Stern. (1999). Hypoxia-associated induction of early growth response-1 gene expression. J Biol Chem 274:15030–15040.
14. Shen N, X Yu, F-Y Pan, X Gao, B Xue and C-J Li. (2011). An early response transcription factor, Egr-1, enhances insulin resistance in type 2 diabetes with chronic hyperinsulinism. J Biol Chem 286:14508–14515.
15. Yu X, N Shen, M-L Zhang, F-Y Pan, C Wang, W-P Jia, C Liu, Q Gao, X Gao, B Xue and C-J Li. (2011). Egr-1 decreases adipocyte insulin sensitivity by tilting PI3K/Akt and MAPK signal balance in mice. EMBO J 30:3754–3765.
16. Pagel J-I and E Deindl. (2012). Disease progression mediated by Egr-1 associated signaling in response to oxidative stress. Int J Mol Sci 13:13104–13117.
17. Kim JN, HJ Kim, SH Jeong, YC Kye and SW Son. (2011). Cigarette smoke-induced early growth response-1 regulates the expression of the cysteine-rich 61 in human skin dermal fibroblasts. Exp Dermatol 20:992–997.
18. Khachigian LM. (2006). Early growth response-1 in cardiovascular pathobiology. Circ Res 98:186–191.
19. Harja E, LG Bucciarelli, Y Lu, DM Stern, YS Zou, AM Schmidt and S-F Yan. (2004). Early growth response-1 promotes atherogenesis: mice deficient in early growth response-1 and apolipoprotein E display decreased atherosclerosis and vascular inflammation. Circ Res 94:333–339.
20. Zhu S, Y Lu, J Zhu, J Xu, H Huang, M Zhu, Y Chen, Y Zhou, X Fan and Z Wang. (2011). Effects of intrahepatic bone-derived mesenchymal stem cells autotransplantation on the diabetic Beagle dogs. J Surg Res 168:213–223.
21. Yeung TY, KL Seeberger, T Kin, A Adesida, N Jomha, AM Shapiro and GS Korbutt. (2012). Human mesenchymal stem cells protect human islets from pro-inflammatory cytokines. PLoS One 7:30.
22. Zuk PA, M Zhu, H Mizuno, J Huang, JW Futrell, AJ Katz, P Benhaim, HP Lorenz and MH Hedrick. (2001). Multilineage cells from human adipose tissue: implications for cell-based therapies. Tissue Eng 7:211–228.
23. Cramer C, E Freisinger, RK Jones, DP Slakey, CL Dupin, ER Newsome, EU Alt and R Izadpanah. (2010). Persistent high glucose concentrations alter the regenerative potential of mesenchymal stem cells. Stem Cells Dev 19:1875–1884.
24. Kimura K, M Nagano, G Salazar, T Yamashita, I Tsuboi, H Mishima, S Matsushita, F Sato, K Yamagata and O Ohneda. (2014). The role of CCL5 in the ability of adipose tissue-derived mesenchymal stem cells to support repair of ischemic regions. Stem Cells Dev 23:488–501.
25. Nagano M, T Yamashita, H Hamada, K Ohneda, K-I Kimura, T Nakagawa, M Shibuya, H Yoshikawa and O Ohneda. (2007). Identification of functional endothelial progenitor cells suitable for the treatment of ischemic tissue using human umbilical cord blood. Blood 110:151–160.
26. Gaiba S, LP Franca, JP Franca and LM Ferreira. (2012). Characterization of human adipose-derived stem cells. Acta Cir Bras 27:471–476.
27. Minteer D, K Marra and JP Rubin. (2012). Adipose-derived mesenchymal stem cells: biology and potential applications. In: *Mesenchymal Stem Cells: Basics and Clinical Application I*. B Weyand, M Dominici, R Hass, R Jacobs, and C Kasper, eds. Springer Berlin Heidelberg, Germany, pp 1–13.
28. Zuk PA, M Zhu, P Ashjian, DA De Ugarte, JI Huang, H Mizuno, ZC Alfonso, JK Fraser, P Benhaim and MH Hedrick. (2002). Human adipose tissue is a source of multipotent stem cells. Mol Biol Cell 13:4279–4295.
29. Tontonoz P, RA Graves, AI Budavari, H Erdjument-Bromage, M Lui, E Hu, P Tempst and BM Spiegelman. (1994). Adipocyte-specific transcription factor ARF6 is a heterodimeric complex of two nuclear hormone receptors, PPAR gamma and RXR alpha. Nucleic Acids Res 22:5628–5634.
30. Diez JJ and P Iglesias. (2003). The role of the novel adipocyte-derived hormone adiponectin in human disease. Eur J Endocrinol 148:293–300.
31. Lee KS, HJ Kim, QL Li, XZ Chi, C Ueta, T Komori, JM Wozney, EG Kim, JY Choi, HM Ryoo and SC Bae. (2000). Runx2 is a common target of transforming growth factor beta1 and bone morphogenetic protein 2, and cooperation between Runx2 and Smad5 induces osteoblast-specific

gene expression in the pluripotent mesenchymal precursor cell line C2C12. Mol Cell Biol 20:8783–8792.
32. Farley JR, JE Wergedal and DJ Baylink. (1983). Fluoride directly stimulates proliferation and alkaline phosphatase activity of bone-forming cells. Science 222:330–332.
33. Von Bauer R, D Oikonomou, A Sulaj, S Mohammed, A Hotz-Wagenblatt, H-J Gröne, B Arnold, C Falk, D Luethje, et al. (2013). CD166/ALCAM mediates proinflammatory effects of S100B in delayed type hypersensitivity. J Immunol 191:369–377.
34. Yan SF, R Ramasamy and AM Schmidt. (2008). Mechanisms of disease: advanced glycation end-products and their receptor in inflammation and diabetes complications. Nat Rev Endocrinol 4:285–293.
35. Olefsky JM. (1976). The insulin receptor: its role in insulin resistance of obesity and diabetes. Diabetes 25:1154–1161.
36. Virolle T, ED Adamson, V Baron, D Birle, D Mercola, T Mustelin and I de Belle. (2001). The Egr-1 transcription factor directly activates PTEN during irradiation-induced signalling. Nat Cell Biol 3:1124–1128.
37. Bouzakri K, M Roques, P Gual, S Espinosa, F Guebre-Egziabher, J-P Riou, M Laville, Y Le Marchand-Brustel, J-F Tanti and H Vidal. (2003). Reduced activation of phosphatidylinositol-3 kinase and increased serine 636 phosphorylation of insulin receptor substrate-1 in primary culture of skeletal muscle cells from patients with type 2 diabetes. Diabetes 52:1319–1325.
38. Sun XJ, P Rothenberg, CR Kahn, JM Backer, E Araki, PA Wilden, DA Cahill, BJ Goldstein and MF White. (1991). Structure of the insulin receptor substrate IRS-1 defines a unique signal transduction protein. Nature 352:73–77.
39. Yan S-F, T Fujita, J Lu, K Okada, Y Shan Zou, N Mackman, DJ Pinsky and DM Stern. (2000). Egr-1, a master switch coordinating upregulation of divergent gene families underlying ischemic stress. Nat Med 6:1355–1361.
40. Wu M, DS Melichian, M de la Garza, K Gruner, S Bhattacharyya, L Barr, A Nair, S Shahrara, PH Sporn, et al. (2009). Essential roles for early growth response transcription factor Egr-1 in tissue fibrosis and wound healing. Am J Pathol 175:1041–1055.
41. Liu C, J Yao, D Mercola and E Adamson. (2000). The transcription factor EGR-1 directly transactivates the fibronectin gene and enhances attachment of human glioblastoma cell line U251. J Biol Chem 275:20315–20323.
42. Bhattacharyya S, F Fang, W Tourtellotte and J Varga. (2013). Egr-1: new conductor for the tissue repair orchestra directs harmony (regeneration) or cacophony (fibrosis). J Pathol 229:286–297.
43. Hasan RN and AI Schafer. (2008). Hemin upregulates Egr-1 expression in vascular smooth muscle cells via reactive oxygen species ERK-1/2-Elk-1 and NF-kappaB. Circ Res 102:42–50.
44. Atkinson S and SB Fox. (2004). Vascular endothelial growth factor (VEGF)-A and platelet-derived growth factor (PDGF) play a central role in the pathogenesis of digital clubbing. J Pathol 203:721–728.
45. You J-J, C-H Yang, M-S Chen and C-M Yang. (2009). Cysteine-rich 61, a member of the CCN family, as a factor involved in the pathogenesis of proliferative diabetic retinopathy. Invest Ophthalmol Vis Sci 50:3447–3455.
46. Doi T, A Mima, T Matsubara, T Tominaga, H Arai and H Abe. (2008). The current clinical problems for early phase of diabetic nephropathy and approach for pathogenesis of diabetic nephropathy. Diabetes Res Clin Pract 13:7.
47. Hayashi Y, H Makino and Z Ota. (1992). Serum and urinary concentrations of type IV collagen and laminin as a marker of microangiopathy in diabetes. Diabet Med 9:366–370.
48. Zhu X, Y Song, R Huo, J Zhang, S Sun, Y He, H Gao, M Zhang, X Sun, et al. (2015). Cyr61 participates in the pathogenesis of rheumatoid arthritis by promoting proIL-1beta production by fibroblast-like synoviocytes through an AKT-dependent NF-kappaB signaling pathway. Clin Immunol 157:187–197.
49. Mauer J, B Chaurasia, J Goldau, MC Vogt, J Ruud, KD Nguyen, S Theurich, AC Hausen, J Schmitz, et al. (2014). Signaling by IL-6 promotes alternative activation of macrophages to limit endotoxemia and obesity-associated resistance to insulin. Nat Immunol 15:423–430.
50. Fontes JA, NR Rose and D Cihakova. (2015). The varying faces of IL-6: From cardiac protection to cardiac failure. Cytokine 74:62–68.
51. Hossain M, MO Faruque, G Kabir, N Hassan, D Sikdar, Q Nahar and L Ali. (2010). Association of serum TNF-α and IL-6 with insulin secretion and insulin resistance in IFG and IGT subjects in a Bangladeshi population. Int J Diabetes Mellitus 2:165–168.
52. Gallucci RM, PP Simeonova, JM Matheson, C Kommineni, Jl Guriel, T Sugawara and MI Luster. (2000). Impaired cutaneous wound healing in interleukin-6–deficient and immunosuppressed mice. FASEB J 14:2525–2531.
53. Liechty KW, NS Adzick and TM Crombleholme. (2000). Diminished interleukin 6 (IL-6) production during scarless human fetal wound repair. Cytokine 12:671–676.
54. Chen S-J, H Ning, W Ishida, S Sodin-Semrl, S Takagawa, Y Mori and J Varga. (2006). The early-immediate gene EGR-1 is induced by transforming growth factor-β and mediates stimulation of collagen gene expression. J Biol Chem 281:21183–21197.
55. Bhattacharyya S, SJ Chen, M Wu, M Warner-Blankenship, H Ning, G Lakos, Y Mori, E Chang, C Nihijima, et al. (2008). Smad-independent transforming growth factor-beta regulation of early growth response-1 and sustained expression in fibrosis: implications for scleroderma. Am J Pathol 173:1085–1099.
56. Lee CG, SJ Cho, MJ Kang, SP Chapoval, PJ Lee, PW Noble, T Yehualaeshet, B Lu, RA Flavell, et al. (2004). Early growth response gene 1-mediated apoptosis is essential for transforming growth factor beta1-induced pulmonary fibrosis. J Exp Med 200:377–389.
57. Kim J-H, DS Choi, O-H Lee, S-H Oh, SM Lippman and H-Y Lee. (2011). Antiangiogenic antitumor activities of IGFBP-3 are mediated by IGF-independent suppression of Erk1/2 activation and Egr-1–mediated transcriptional events. Blood 118:2622–2631.

Address correspondence to:
Dr. Osamu Ohneda
Laboratory of Regenerative Medicine and Stem Cell Biology
University of Tsukuba
1-1-1 Tennodai
Tsukuba 305-8575
Japan

E-mail: oohneda@md.tsukuba.ac.jp

Received for publication October 18, 2015
Accepted after revision March 17, 2016
Prepublished on Liebert Instant Online March 17, 2016